International Journal of Heat and Mass Transfer 114 (2017) 1350–1356

Contents lists available at ScienceDirect

International Journal of Heat and Mass Transfer

journal homepage: www.elsevier.com/locate/ijhmt

Review

Entrance-length dendritic plate heat exchangers

A. Bejan [a,*], M. Alalaimi [b], A.S. Sabau [c], S. Lorente [d]

[a] Duke University, Durham, NC 27708-0300, USA
[b] Kuwait University, Box 5969, Safat 13060, Kuwait
[c] Oak Ridge National Laboratory, Oak Ridge, TN 37830, USA
[d] Université de Toulouse, INSA, 135 Avenue de Rangueil, 31077 Toulouse, France

ARTICLE INFO

Article history:
Received 28 March 2017
Received in revised form 19 June 2017
Accepted 21 June 2017
Available online 17 July 2017

Keywords:
Constructal
Evolution
Scaling up
Dendritic
Entrance length
Heat exchanger

ABSTRACT

Here we explore the idea that the highest heat transfer rate between two fluids in a given volume is achieved when plate channel lengths are given by the thermal entrance length, i.e., when the thermal boundary layers meet at the exit of each channel. The overall design can be thought of an elemental construct of a dendritic heat exchanger, which consists of two tree-shaped streams arranged in cross flow. Every channel is as long as the thermal entrance length of the developing flow that resides in that channel. The results indicate that the overall design will change with the total volume and total number of channels. We found that the lengths of the surfaces swept in cross flow would have to decrease sizably as number of channels increases, while exhibiting mild decreases as total volume increases. The aspect ratio of each surface swept by fluid in cross flow should be approximately square, independent of total number of channels and volume. We also found that the minimum pumping power decreases sensibly as the total number of channels and the volume increase. The maximized heat transfer rate per unit volume increases sharply as the total volume decreases, in agreement with the natural evolution toward miniaturization in technology.

Contents

1. Technology evolution

Technology evolution [1,2] is emerging as the most common manifestation of the universal tendency toward evolutionary design in nature, which in physics is summarized as the constructal law. Technology evolves visibly in our lifetime, and reveals the physics meaning of the evolution phenomenon: evolution means changes that occur freely in a flow architecture over time, in a discernable direction in time from the point of view of the observer. The movie tape of evolutionary images runs in one direction, forward. Think of evolution as the phenomenon of geometric irreversibility.

The physics of evolution had its start in engineering [2,3]. Since 1996, this physics phenomenon and law have guided theoretical and applied investigations that feed an active field that continues to grow. To review the field is not the present objective, because

* Corresponding author.
E-mail address: abejan@duke.edu (A. Bejan).

http://dx.doi.org/10.1016/j.ijheatmasstransfer.2017.06.094
0017-9310/

Nomenclature

a,b,c	thicknesses, m
C	costs, Eq. (43)
D	transversal dimension, m
f_1	factor, Eq. (1)
H	height, m, Fig. 1
k	fluid thermal conductivity, W m^{-1} K^{-1}
L	length, m, Fig. 1
L_{flow}	flow length, m
L_{long}	long side of cross section, m
L_{scale}	length scale, m
K	local pressure loss factor, Eq. (48)
$K_{P,HT}$	relative cost factors, Eqs. (45) and (46)
$\dot{m}$	mass flow rate, kg s^{-1}
n	number of channels
$\tilde{P}$	pumping power, dimensionless, Eq. (26)
Pr	Prandtl number
q	heat transfer rate, W
r	factor, Eq. (28)
Re_D	Reynolds number
t	wall thickness, m
T	temperature, K
U	mean velocity, m s^{-1}
V	volume, m^3
W	spacing, m, Fig. 1
$\dot{W}$	pumping power, W
X	length, m, Fig. 1

Greek symbols

ΔT	temperature difference, K
η	aspect ratio, X/L
μ	viscosity, kg s^{-1} m^{-1}
ν	kinematic viscosity, m^2 s^{-1}
ξ	aspect ratio, H/L
σ	solid volume fraction

Superscript

$\tilde{()}$	dimensionless

Subscript

HT	heat transfer
M	material
P	pumping
TOT	total

reviews appear regularly in the literature. There are two objectives in this article:

The first objective is to draw attention to the rapid growth of the evolutionary design field toward industrial applications. Advances are published regularly for heat exchangers [4–13], fuel cells [14], fluid networks [15–20], steam generators [21,22], fluid channels [23–27], energy storage [28], transportation [29–32], power generation [33–37], and management [38].

The second objective is to project on this background the concept of constructal dendritic heat exchanger [4,5], and to propose a conceptual advance in design, which applies at all scales, in every channel. For example, the concept proposed here is relevant to the design of evaporator heat exchangers for the geothermal industry, in which currently shell-and-tube types are used. Novel heat exchangers are needed to increase the brine effectiveness and decrease the costs of geothermal power generation.

2. Entrance-length channels

Recent advances in constructal design indicate that a flow channel packs maximum heat transfer density when the wall boundary layers meet at the channel exit (for a review, see Ref. 39). This holds for forced convection and natural convection in both laminar and turbulent regimes. This design feature means that the length of the flow channel must match the entrance length of the flow.

Another way to recognize this design rule is to recognize that the channel dimensions must be fitted to the length scales of the flow that fills the channel. The length scale of the flow field is the thickness of the boundary layer that develops along each surface, downstream from the entrance. For clarity, assume that the velocity boundary layer is nearly as thick as the thermal boundary layer, which means that $Pr \sim 1$. The longitudinal flow length where the boundary layers of opposing surfaces merge is the entrance length. If the actual length of the channel is shorter than the entrance length, then the core of the flow does not participate in convecting heat from the walls, and the channel volume is not 'packed' as densely as possible with heat flow. In the opposite extreme, when the channel length is much greater than the entrance length, most of the volume is filled with fluid that has already been heated or cooled by the walls, exhibiting much lower heat transfer rates from the walls. The maximum heat transfer rate per unit volume belongs to the design located at the *intersection of asymptotes* [39], which is the design with flows that sweep solid surfaces as long as the entrance length of the flow itself.

The flow structure with channels as long as the entrance length differs sensibly from other structures. We showed this fact in the design of a T-shaped construct of two round tubes [40], one stem (D_1, L_1) and two branches (D_2, L_2), on a fixed area ($2L_2L_1$) and subject to fixed total tube volume. When the flow is laminar and fully developed in every tube, the architecture with the smallest overall pressure drop (or smallest pumping power) is characterized by the aspect ratios $D_1/D_2 = 2^{1/3}$ and $L_1/L_2 = 2^{1/3}$. If we add the requirement to maximize the volumetric heat transfer rate, which means that L_1 and L_2 are the entrance lengths of the stem and the branches, the optimal ratio L_1/L_2 becomes 2. The design for minimum pumping power and maximum heat transfer density, simultaneously, is characterized by $D_1/D_2 = 2^{1/3}$ and $L_1/L_2 = 2$, not by $D_1/D_2 = 2^{1/3}$ and $L_1/L_2 = 2^{1/3}$.

3. Dendritic cross-flow plate heat exchanger

In this paper, we show how the entire architecture of a three-dimensional cross-flow plate heat exchanger is determined as a consequence that in every one of its channels, large or small, the channel length scale matches the flow entrance length scale. Specifically, the cross-flow plate heat exchanger shown in Fig. 1 is considered in this paper. Cold fluid ($\dot{m}$) enters from the left through a channel of length L, width H, and spacing a. The stream is distributed to its left side to n parallel-plates channels, each of length X, spacing W, width H, and mass flow rate $\dot{m}/n$.

Fig. 1 is a dendritic flow architecture because it consists of two combs perpendicular to each other, with their bristles in cross flow. The hot stream is one comb, and the cold stream is the other comb. Each comb is a tree with branches on one side only. Previously, we evolved the constructal design of two flow combs matched tip to tip, in the same plane, with application to vasculatures for self-healing and self-cooling (Ref. [40], ch. 8). In Fig. 1, the planes of the two sets of bristles are perpendicular. The first work of this

kind was on two flow combs 'interdigitated' in the same plane [2,41].

To start, assume that in every channel the flow and heat transfer are by laminar forced convection, and the working fluids under consideration have constant transport properties and Prandtl numbers comparable to 1. Thus, along the entrance length the velocity boundary layer thickness is essentially the same as the thermal boundary layer thickness. For two parallel walls of flow length L_{flow} and spacing D, the classical result for the flow entrance length is (cf. Ref. [39], Section 3.1)

$$\frac{L_{flow}}{D} \sim f_1 Re_D \tag{1}$$

where $Re_D = UD/\nu$ and the factor f_1 is of order 10^{-2}. Considering that the fluid mean velocity is $U = \dot{m}/(\rho D L_{long})$, where $\dot{m}$ is the mass flow rate, and L_{long} is the long side of the flat rectangular (slit) cross section of the channel, Eq. (1) becomes:

$$\frac{L_{flow}}{D} \sim f_1 \frac{\dot{m}}{\mu L_{long}} \tag{2}$$

Oriented in cross-flow is the warm stream ($\dot{m}$), which is shown flowing vertically in Fig. 1. The warm stream flows through n channels, each of flow length H, spacing b, width X, and mass flow rate $\dot{m}/n$. For the large cold channel (LaH), Eq. (2) states that

$$\frac{L}{a} \sim f_1 \frac{\dot{m}}{\mu H} \tag{3}$$

Similarly, for the large warm channel (LcX) we write

$$\frac{L}{c} \sim f_1 \frac{\dot{m}}{\mu X} \tag{4}$$

For each of the n branches of this channel, Eq. (2) requires

$$\frac{X}{W} \sim f_1 \frac{\dot{m}}{n\mu H} \tag{5}$$

For each of the n warm channels, we write similarly

$$\frac{H}{b} \sim f_1 \frac{\dot{m}}{n\mu X} \tag{6}$$

The dimensions of this three-dimensional construct are related through two geometric constraints,

$$n(b + W) = L \tag{7}$$

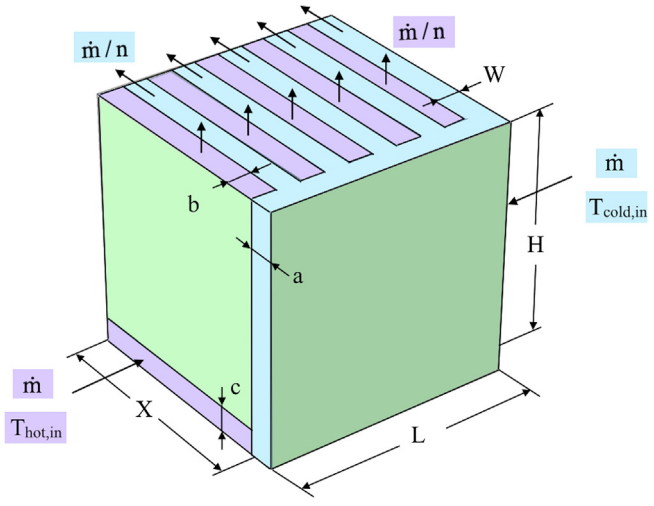

Fig. 1. Three-dimensional flow construct with two streams in cross flow.

$$L(H + c)(X + a) = V \tag{8}$$

where V is the specified volume of the construct.

To summarize, the construct is described by eight dimensions (L, H, X, a, b, c, W, n) and six equations, Eqs. (3)–(8), which means that it has two degrees of freedom. Next, Eqs. (3)–(8) are placed in dimensionless form by recognizing on the right side of Eqs. (3)–(5) the length scale

$$L_{scale} \sim f_1 \frac{\dot{m}}{\mu} \tag{9}$$

and defining the dimensionless variables

$$(\tilde{L}, \tilde{a}, \tilde{b}, \tilde{c}, \tilde{W}, \tilde{X}) = (L, a, b, c, W, X)/L_{scale} \tag{10}$$

$$\tilde{V} = V/L_{scale}^3 \tag{11}$$

Eqs. (3)–(8) reduce to six dimensionless equations

$$\xi \frac{\tilde{L}^2}{\tilde{a}} = 1 \tag{12}$$

$$\eta \frac{\tilde{L}^2}{\tilde{c}} = 1 \tag{13}$$

$$\xi n \frac{\tilde{X}\tilde{L}}{\tilde{W}} = 1 \tag{14}$$

$$\xi n \frac{\tilde{X}\tilde{L}}{\tilde{b}} = 1 \tag{15}$$

$$n(\tilde{b} + \tilde{W}) = \tilde{L} \tag{16}$$

$$\tilde{L}(\xi\tilde{L} + \tilde{c})(\eta\tilde{L} + \tilde{a}) = \tilde{V} \tag{17}$$

where ξ and η are the two aspect ratios of the three dimensional body,

$$\xi = \frac{H}{L} \quad \eta = \frac{X}{L} \tag{18}$$

Assuming that $X \gg a$, and $H \gg c$, such that Eq. (8) is replaced by $V \cong XLH$, the solution to this system of equations is:

$$\tilde{L} = \left(\frac{\tilde{V}}{\xi\eta}\right)^{1/3} \tag{19}$$

$$\tilde{a} = \xi^{1/3}\eta^{-2/3}\tilde{V}^{2/3} \tag{20}$$

$$\tilde{b} = n\xi^{1/3}\eta^{1/3}\tilde{V}^{2/3} \tag{21}$$

$$\tilde{c} = \xi^{-2/3}\eta^{1/3}\tilde{V}^{2/3} \tag{22}$$

$$\tilde{W} = n\xi^{1/3}\eta^{1/3}\tilde{V}^{2/3} \tag{23}$$

For identical working fluids, b = W as shown in Eqs. (21) and (23). The validity domain of the simplifying assumptions, $X \gg a$, and $H \gg c$, will be discussed at the end of Section 5.

4. Pumping power

The pumping power required by the device is the sum of three penalties, each of the form $(\dot{m}/\rho)\Delta P$, where $\dot{m}$ and ΔP are the mass flow rate and pressure drop of the particular channel. There are four channel sizes, indicated in Fig. 1 by the spacings a, c, W and b. Each pressure drop for laminar flow over a length comparable with the entrance length has the same scale as for fully developed flow (cf. Ref. [39], pp. 130–132),

$$\Delta P \sim \nu \frac{(\text{length of channel})(\text{mass flow rate})}{(\text{spacing})^4} \tag{24}$$

In sum, the total pumping power requirement ($\tilde{P}$) reduces to the dimensionless expression

$$\frac{\dot{W}\rho L_{scale}^3}{\nu \dot{m}^2} \sim \frac{\tilde{L}}{\tilde{a}^4} + \frac{\tilde{X}}{n^2\tilde{W}^4} + \frac{\tilde{L}}{\tilde{c}^4} + \frac{\tilde{H}}{n^2\tilde{b}^4} = \tilde{P} \tag{25}$$

where the four terms account, in order, for the channels of spacings a, W, c and b. In view of the solution (19)–(23), Eq. (25) becomes

$$\tilde{P} = \frac{\eta^{7/3}}{\xi^{5/3}\tilde{V}^{7/3}} + \frac{1}{n^6\xi^{5/3}\eta^{2/3}\tilde{V}^{7/3}} + \frac{\xi^{7/3}}{\eta^{5/3}\tilde{V}^{7/3}} + \frac{16n^2\xi^2\eta}{r^4\tilde{V}} \tag{26}$$

The factor r is shorthand for

$$r = \frac{2b}{b+W} = 2(1 - n^2\xi^{2/3}\eta^{2/3}\tilde{V}^{1/3}) \tag{27}$$

which is approximately equal to 1 when the channel spacings b and W are comparable in size.

The right side of Eq. (26) is a dimensionless function of four variables, $\tilde{P}(\xi, \eta, n, \tilde{V})$, which is proportional to the pumping power required by the whole construct, Fig. 1. We studied the behavior of this function by first assuming $\tilde{V} = 1$ and n = 4, and then varying one parameter, for example η, while holding ξ fixed, as shown in Fig. 2. The condition r > 0 is satisfied by the (ξ, η) range covered in this figure.

Each curve reveals a minimum, $\tilde{P}_m$, which is reached at a value η_{opt} that depends on the assumed value of ξ. These results are summarized in Fig. 3 where, again, $\tilde{V} = 1$ and n = 4. The $\tilde{P}_m$ curve shown in Fig. 3 has its own minimum ($\tilde{P}_{mm} \cong 3.61$) at $\xi_{opt} \cong 0.061$, which corresponds to $\eta_{opt} \cong 0.052$. These three values, $\tilde{P}_{mm}$, ξ_{opt} and η_{opt}, are the results that we record for the assumed parameters n = 4 and $\tilde{V} = 1$. Next, we repeated the procedure of Figs. 2 and 3 for other $(n, \tilde{V})$ pairs. First, we kept $\tilde{V} = 1$, and used larger n values, such as 8 and 16. Fig. 4 shows how the solution ($\tilde{P}_{mm}$, ξ_{opt}, η_{opt}) varies with n for constant $\tilde{V}$ values.

Finally, we repeated the entire procedure of Figs. 2–4 for additional values of $\tilde{V}$. The results that emerged in Fig. 4 shows how the

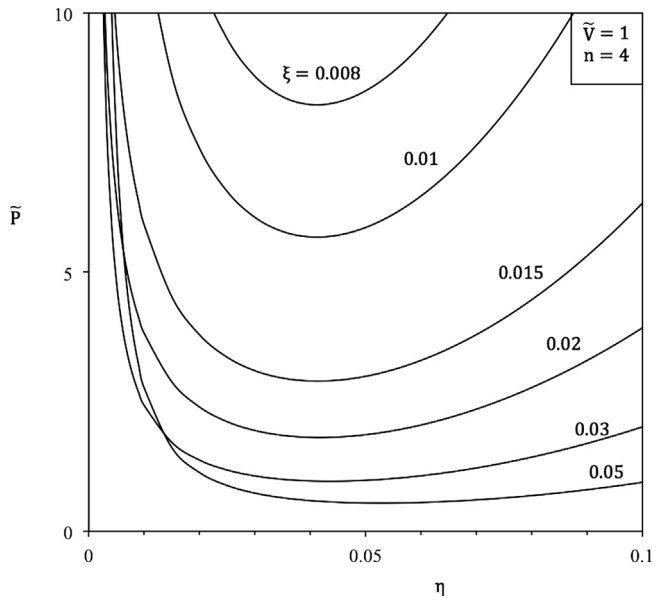

Fig. 2. The minimization of the overall pumping power requirement $\tilde{P}$ versus η, at fixed $(\xi, n, \tilde{V})$.

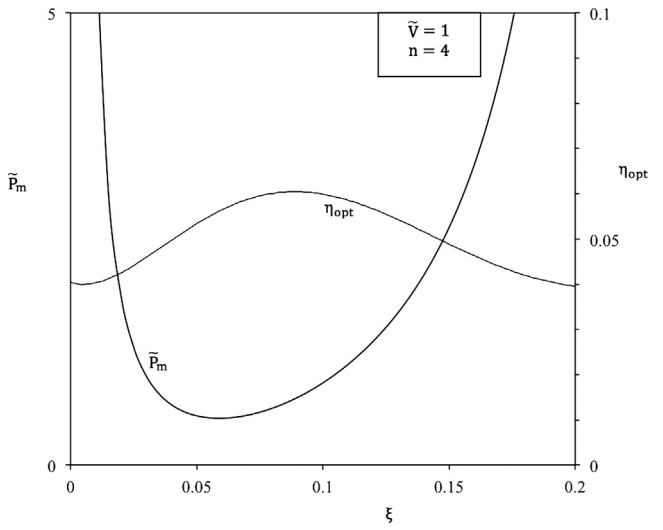

Fig. 3. Further minimization of the minimized pumping power requirement ($\tilde{P}_m$) by varying ξ at fixed $(n, \tilde{V})$.

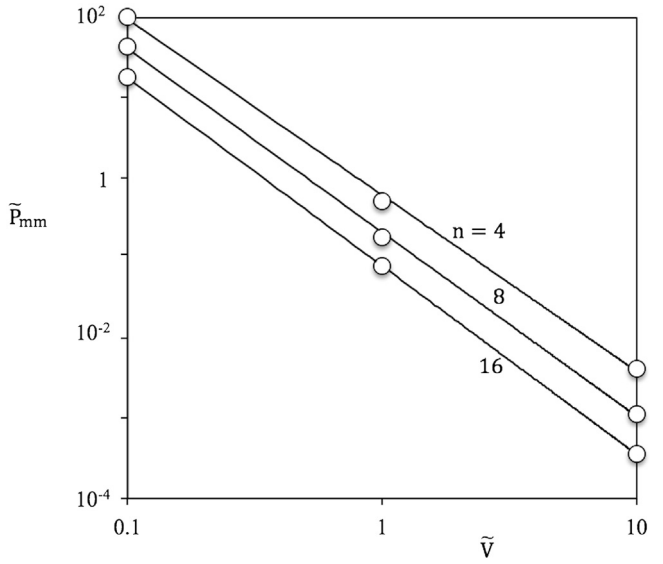

Fig. 4. The twice-minimized pumping power ($\tilde{P}_{mm}$) and the optimal shape of the three-dimensional construct (ξ_{opt}, η_{opt}) for assumed values of n and $\tilde{V}$.

solution ($\tilde{P}_{mm}$, ξ_{opt}, η_{opt}) depends on both n and $\tilde{V}$. The results are correlated as power laws,

$$\tilde{P}_{mm} = (4.06 \pm 0.75)n^{-1.4}\tilde{V}^{-2.3} \tag{28}$$

$$\xi_{opt} = (0.5 \pm 0.08)n^{-1.6}\tilde{V}^{-0.18} \tag{29}$$

$$\eta_{opt} = (0.31 \pm 0.057)n^{-1.4}\tilde{V}^{-0.24} \tag{30}$$

Worth noting is that the ξ_{opt} and η_{opt} correlations are similar with respect to the effect of n and $\tilde{V}$. Indeed, the power-law correlation of the values of the ratio η_{opt}/ξ_{opt} shows a very weak dependence on n and $\tilde{V}$:

$$\left(\frac{\eta}{\xi}\right)_{opt} = (0.66 \pm 0.1)n^{0.18}\tilde{V}^{-0.06} \tag{31}$$

For the $(n, \tilde{V})$ range covered by the present results, the ratio $(\eta/\xi)_{opt}$ is practically constant and of order 1. The scaling result

$\eta_{opt} \sim \xi_{opt}$ translates into a rule of geometric similarity for all entrance-length heat exchangers, large or small:

$$H \sim X \tag{32}$$

This means that the surfaces swept by the cross flow of mini-streams ($\dot{m}/n$) should be square for the case of a balanced heat exchanger.

5. Heat transfer

The heat transfer rate between the two streams $\dot{m}$ in cross flow can be determined via scale analysis. The scale of the local temperature difference across any heat transfer surface element is set by the difference between the two inlet temperatures, $\Delta T = T_{hot,in} - T_{cold,in}$. The heat flux scale is $q'' \sim k\Delta T/W \sim k\ \Delta T/b$. The surfaces of the small channels add up to 2nXH. The spots of the large cold channel (LaH) that come in contact with warm channels contribute the contact surface nbH. The total heat transfer rate between the two streams is

$$q \sim (2nXH + nbH)k\frac{\Delta T}{W} \tag{33}$$

The second term in parentheses is negligible when $b < 2X$, and after using $W = L/n$ and Eqs. (29) and (30), the q expression (33) becomes

$$\frac{q}{2k\Delta TL_{scale}} \cong 0.3\tilde{V}^{0.05} \tag{34}$$

This shows that the total heat transfer rate in the 'entrance length' design is essentially independent of n and $\tilde{V}$.

The corresponding result for the heat transfer density q/V is

$$\frac{q/V}{2k\Delta T/L_{scale}^2} \cong 0.3\tilde{V}^{-0.95} \tag{35}$$

In conclusion, the maximized heat transfer density is insensitive to n, and increases sensibly as the size (V) decreases. In other words, this design shows that the trend toward *miniaturization* should be expected, in accord with other evolutionary designs that define the constructal-law field [1]. This conclusion holds for $b < 2X$, which after using Eqs. (21), (29) and (30) translates into $n^{1.2}\tilde{V}^{0.88} \lesssim 10$. In other words, when n is of order 10, $\tilde{V}$ must be smaller than 1, i.e., toward the left side of the data plotted in Fig. 4.

6. Material volume

In most studies on novel heat exchangers the pumping costs are considered equal to the overall cost of the heat exchanger, neglecting the cost of the material and construction [42]. For a thorough design study of the dendritic object (Fig. 1) the material costs are investigated in this section. The expense is directly proportional to the amount of material. For applications in geothermal power generation, the heat exchangers are made of carbon steel or duplex stainless steel at a cost that cannot be simply neglected. The amount of this alloy material is a key parameter that follows from the dimensions determined above.

Under the approximations $c \ll H$ and $a \ll X$, the total volume is $V = LHX$, and the volume of solid material is

$$\frac{V_s}{t} = (2n+1)HX + n(bH + WX) \tag{36}$$

where t is the thickness of the wall that separates two adjacent channels. Assume that t is a known constant, and note that t must satisfy the inequalities $t \ll b$ and $t \ll W$.

The ratio $\sigma = V_s/V$ is the solid volume fraction (the 'solidity') of the structure determined in Fig. 1. Its value is estimated by using Eqs. (19), (29) and (30) for $\tilde{L}$, ξ and η. The resulting expression is

$$\sigma = 2\tilde{t}\tilde{V}^{-0.473} \tag{37}$$

where $\tilde{t} = t/L_{scale}$. The σ value must meet two conditions simultaneously. First, σ must be smaller than 1, and this places a condition that the wall thickness must satisfy:

$$\tilde{t} < \frac{1}{2}\tilde{V}^{0.473} \tag{38}$$

In view of the conclusion that $\tilde{V}$ must be smaller than 1, reached at the end of Section 5, Eq. (38) requires $\tilde{t}$ to be smaller than 1 as well.

Second, recall that t must be smaller than both b and W. Writing $t < (b, W)$ and using Eqs. (21) and (23), we obtain

$$\tilde{t} < n\xi^{1/3}\eta^{1/3}\tilde{V}^{2/3} \tag{39}$$

which after using Eqs. (29) and (30) reduces to

$$\sigma < 0.577\tilde{V}^{0.053} \tag{40}$$

Because $\tilde{V}$ is smaller than 1, the solidity σ is also smaller than 1. In summary, the calculation of the solid volume fraction of the dendritic construct is consistent with the $\tilde{V}$ domain of validity of the dimensions developed in Sections 3–5. For the thermoeconomics analysis developed next, it is sufficient to account for the material volume as the product σV, where σ is a known constant factor smaller than 1.

There are two additional costs that compete with the cost of the amount of material. One is the pumping power $\dot{W}_P$, which after Eqs. (9), (26) and (28) scales as

$$\dot{W}_P \sim \frac{\nu\mu^3}{\rho\dot{m}}n^{-1.4}\tilde{V}^{-2.3} \tag{41}$$

The other cost is the loss of useful power associated with the heat transfer irreversibility of q flowing across the temperature gap ΔT, namely $\dot{W}_{HT} = q\Delta T/T$, where T is the thermodynamic temperature level at which the device functions. After using Eqs. (9) and (29) and neglecting constant dimensionless factors, the heat-transfer power loss becomes

$$\dot{W}_{HT} \sim \frac{q^2\mu}{kT\dot{m}}\tilde{V}^{-0.05} \tag{42}$$

Noteworthy is that $\dot{W}_P$ and $\dot{W}_{HT}$ are smaller when the device is larger. This is the universal physics phenomenon of economies of scale [43,44], and it is more pronounced in the behavior of $\dot{W}_P$ with respect to the size $\tilde{V}$. This trend is oriented against the behavior of the cost of material, which increases with $\tilde{V}$. In future applications of the dendritic design concept this conflict is the trade off from which emerges the size $\tilde{V}$ for which the total cost (material, $\dot{W}_P$, $\dot{W}_{HT}$) is minimal. To complete this thermoeconomics optimization calculation [42], one has to assign appropriate per-unit costs to the material amount σV, $\dot{W}_P$ and $\dot{W}_{HT}$,

$$C_{TOT} = C_M\sigma V + C_P\dot{W}_P + C_{HT}\dot{W}_{HT} \tag{43}$$

where C_M, C_P and C_{HT} are per-unit costs, and C_{TOT} is the total cost. In dimensionless form, Eq. (4) reads

$$\frac{C_{TOT}}{C_M\sigma L_{scale}^3} = \tilde{V} + K_P n^{-1.4}\tilde{V}^{-2.3} + K_{HT}\tilde{V}^{-0.05} \tag{44}$$

where

$$K_P = \frac{C_P\nu\mu^3}{C_M\sigma L_{scale}^3\rho\dot{m}} \tag{45}$$

$$K_{HT} = \frac{C_{HT} q^2 \mu}{C_M \sigma L_{scale}^3 k T \dot{m}} \tag{46}$$

In Eq. (44), the dominant effect on the total cost is due to the size changes in the first two terms. Approximating that the third term is constant in the $\tilde{V}$ range of interest, and minimizing the total cost by varying V we obtain the 'thermoeconomic' size of the flow system:

$$\tilde{V}_{size} = 1.3 K_p^{0.3} n^{-0.42} \tag{47}$$

7. Concluding remarks

The fundamental aspect of this constructal design is that "scaling-up" does not consist of magnifying (multiplying by the same factor) all the dimensions of the small design. It means to know the physics principle that governs the small design, and to use the same principle to morph, to evolve, and to discover the architecture of the larger design.

The main conclusion is that we should expect the design to change as the size (V) changes, and as the complexity (n) changes. For example, the lengths of the surfaces swept in cross flow (H/L and X/L) should decrease sizably as n increases, while exhibiting mild decreases as V increases. The aspect ratio of each surface swept by fluid in cross flow should be approximately square, independent of n and V. The minimum pumping power ($\dot{W}$) decreases sensibly as n and V increase. The maximized heat transfer rate per unit volume increases sharply as the size (V) decreases. This trend is in accord with the constructal-law evolution toward miniaturization in technology [1].

Looking ahead, the design concept proposed in this paper can be refined further by taking into account the effect of local pressure losses, which was neglected in Section 4. According to Ref. [40] (p. 13), the local pressure loss on a channel that undergoes an abrupt chance (contraction, expansion, elbow, junction) is

$$\Delta P_{local} = K \frac{1}{2} \rho U^2 \tag{48}$$

where K is a dimensionless factor of order 10^{-1}, and U is the mean fluid velocity in the channel. If the channel has the flow length L_{flow} and hydraulic diameter D_h, the pressure loss distributed along the channel (which was taken into account in Section 4) is

$$\Delta P_{distributed} = f \frac{4 L_{flow}}{D_h} \frac{1}{2} \rho U^2 \tag{49}$$

The local pressure loss is smaller than the distributed pressure loss when, after dividing Eq. (48) by Eq. (49), and using the dimensions of the channel of length X and spacing W (or H and b, for the other stream),

$$\frac{K 2W}{f 4X} < 1 \tag{50}$$

This inequality can be rewritten in terms of the results of the present study, i.e., by using in order Eqs. (18), (19), (23), (29) and (30), and writing that for a channel between parallel plates the friction factor is $f = 24/Re_{D_h}$. The inequality (50) becomes

$$Re_{D_h} n^{0.4} \tilde{V} \lesssim \frac{52}{K} \tag{51}$$

where the right hand side is of order 500. This inequality establishes the domain of validity of the assumption that local pressure losses are negligible. This assumption becomes more accurate as Re_{D_h}, n and $\tilde{V}$ decrease individually or together. For example, if $\tilde{V} = 0.1$ (Fig. 4) and n = 10, local pressure losses can be neglected when Re_{D_h} is less than 2000, which covers the entire laminar flow regime. If the volume size is larger, $\tilde{V} = 1$, then local pressure losses are negligible when $Re_{D_h} < 200$, which represents the regime of operation of low Reynolds number heat exchangers.

Conflict of interest

The authors declare that there is no conflict of interest.

Acknowledgement

This work was performed for the project "Freeform Heat Exchangers for Binary Geothermal Power Plants" sponsored by the Geothermal Technologies Program, Office of Energy Efficiency and Renewable Energy, U.S. Department of Energy under contract DE-AC05-00OR22725, Oak Ridge National Laboratory, managed and operated by UT-Battelle, LLC. Mr. Alalaimi's work was supported by Kuwait University. Prof. Bejan's work was also supported by the National Science Foundation.

Notice: This submission was sponsored by a contractor of the United States Government under contract DE-AC05-00OR22725 with the United States Department of Energy. The United States Government retains and the publisher, by accepting the article for publication, acknowledges that the United States Government retains a non-exclusive, paid-up, irrevocable, world-wide license to publish or reproduce the published form of this manuscript, or allow others to do so, for United States Government purposes. The Department of Energy will provide public access to these results of federally sponsored research in accordance with the DOE Public Access Plan (http://energy.gov/downloads/doe-public-access-plan).

References

[1] A. Bejan, The Physics of Life: The Evolution of Everything, St. Martin's Press, New York, 2016.
[2] A. Bejan, Evolution in thermodynamics, Appl. Phys. Rev. 4 (2017) 011305.
[3] A. Bejan, Shape and Structure, from Engineering to Nature, Cambridge University Press, Cambridge, UK, 2000.
[4] A. Bejan, Dendritic constructal heat exchanger with small-scale crossflows and larger-scales counterflows, Int. J. Heat Mass Transfer 45 (2002) 4607–4620.
[5] V.A.P. Raja, T. Basak, S.K. Das, Thermal performance of a multi-block heat exchanger designed on the basis of Bejan's constructal theory, Int. J. Heat Mass Transfer 51 (2008) 3582–3594.
[6] K. Manjunath, S.C. Kaushik, Entropy generation and thermo-economic analysis of constructal heat exchanger, Heat Transfer – Asian Res. 43 (2014) 39–60.
[7] A.V. Azad, M. Amidpour, Economic optimization of shell and tube heat exchanger based on constructal theory, Energy 36 (2011) 1087–1096.
[8] G. Lorenzini, C. Biserni, A vapotron effect application for electronic equipment cooling, J. Electron. Packag. 125 (2003) 475–479.
[9] G. Lorenzini, C. Biserni, L.A.O. Rocha, Geometric optimization of X-shaped cavities and pathways according to Bejan's theory: comparative analysis, Int. J. Heat Mass Transf. 73 (2014) 1–8.
[10] J. Yang, S.-R. Oh, W. Liu, Optimization of shall-and-tube heat exchangers using a general design approach motivated by constructal theory, Int. J. Heat Mass Transfer 77 (2014) 1144–1154.
[11] K. Manjunath, S.C. Kaushik, Second law thermodynamic study of heat exchangers: a review, Renew. Sustain. Energy Rev. 40 (2014) 348–374.
[12] C. Biserni, F.L. Dalpiaz, T.M. Fagundes, L.A.O. Rocha, Constructal design of T-shaped morphing fins coupled with trapezoidal basement: a numerical investigation by means of exhaustive search and genetic algorithm, Int. J. Heat Mass Transf. 109 (2017) 73–81.
[13] J. Yang, A. Fan, W. Liu, A.M. Jacobi, Optimization of shell-and-tube heat exchangers confirming to TEMA standards with designs motivated by constructal theory, Energy Convers. Manage. 78 (2014) 468–476.
[14] G. Lepage, G. Perrier, J. Ramousse, G. Merlin, First steps toward a constructal microbial fuel cell, Biores. Technol. 162 (2014) 123–128. http://dx.doi.org/10.1016/j.biortech.2014.03.139.
[15] Y. Chen, Z. Deng, Gas flow in micro tree-shaped hierarchical network, Int. J. Heat Mass Transfer 80 (2015) 163–169.
[16] E. Cetkin, Constructal vascularized structures, Open Eng. 5 (2015) 220–228.
[17] A.F. Miguel, A study of entropy generation in tree-shaped flow structures, Int. J. Heat Mass Transfer 92 (2016) 349–359.
[18] H.-F. Huang, S.-Y. Liu, W. Guo, A hierarchical tree shaped power distribution network based on constructal theory for EBG structure power plane, Progress Electromag. Res. B 36 (2012) 173–191.
[19] L. Wang, Y. Fan, L. Luo, Lattice Boltzmann method for shape optimization of fluid distributor, Comput. Fluids 94 (2014) 49–57.

[20] J. Kou, Y. Chen, X. Zhou, H. Lu, F. Wu, J. Fan, Optimal structure of tree-like branching networks for fluid flow, Physica A 393 (2014) 527–534.
[21] E. Narouzi, M. Amidpour, Optimal thermodynamic and economic volume of a heat recovery steam generator by constructal design, Int. Comm. Heat Mass Transfer 39 (2012) 1286–1292.
[22] E. Narouzi, M. Mehrgoo, M. Amidpour, Geometric and thermodynamic optimization of a heat recovery steam generator: a constructal design, J. Heat Transfer 134 (2012) 111801.
[23] M.S. Razavi, E. Shirani, M.R. Salimpour, Development of a general method for obtaining the geometry of microfluidic networks, AIP Adv. 4 (2014) 017109.
[24] M.M. Awad, A review of entropy generation in microchannels, Adv. Mech. Eng. 7 (6) (2015) 1–32.
[25] F. Zhang, B. Sundén, W. Zhang, G. Xie, Constructal parallel-flow and counterflow microchannel heat sinks with bifurcations, Numer. Heat Transfer A 68 (2015) 1087–1105.
[26] L. Wang, W. Wu, X. Li, Numerical and experimental investigation of mixing characteristics in the constructal tree-shaped microchannel, Int. J. Heat Mass Transfer 67 (2013) 1014–1023.
[27] M.R. Salimpour, A. Menbari, Analytical optimization of constructal channels used for cooling a ring shaped body based on minimum flow and thermal resistances, Energy 81 (2015) 645–651.
[28] A. Sciacovelli, F. Gagliondi, V. Verda, Maximization of performance of a PCM latent heat storage system with innovative fins, Appl. Energy 137 (2015) 707–715.
[29] N. Shah, S. Kumar, F. Bastani, I.-L. Yen, Optimization models for assessing the peak capacity utilization of intelligent transportation systems, Eur. J. Oper. Res. 216 (2012) 239–251.
[30] M. Trancossi, A response to industrial maturity and energetic issue: a possible solution based on constructal law, Eur. Transp. Res. Rev. 7 (2015) 2, http://dx.doi.org/10.1007/s12544-014-0150-4.
[31] M. Trancossi, A. Dumas, M. Madonia, Optimization of airships with constructal design for efficiency method, SAE Int. 17 (September 2013), http://dx.doi.org/10.4271/2013-01-2168.
[32] A. Dumas, M. Madonia, M. Trancossi, D. Vucinic, Propulsion of photovoltaic cruiser-feeder airships dimensioning by constructal design for efficiency method, SAE Int. 17 (September 2013), http://dx.doi.org/10.4271/2013-01-2303.
[33] G.A. Ledezma, R.S. Bunker, The optimal distribution of pin fins for blade tip cap underside cooling, J. Turbomach. 137 (2015) 011002.
[34] X. Zhou, Y. Xu, S. Yuan, R. Chen, B. Song, Pressure and power potential of sloped-collector solar updraft tower power plant, Int. J. Heat Mass Transfer 75 (2014) 450–461.
[35] P. Botsaris, An approach of the spatial planning of a photovoltaic park using Constructal Theory, Sustain. Energy Technol. Assess. 11 (2015) 11–16.
[36] F. Yao, Y. Chen, G.P. Peterson, Hydrogen production by methanol steam reforming in a disc microreactor with tree-shaped flow architectures, Int. J. Heat Mass Transfer 64 (2013) 418–425.
[37] A. Goldberg, E. Vitkin, G. Linshiz, S.A. Khan, N.J. Hillson, Z. Yakhini, M.L. Yarmush, Proposed design of distributed macroalgal refineries: thermodynamics, bioconversion technology, and sustainability implications for developing economies, Biofuels, Bioprod. Bioref. 8 (2014) 67–82.
[38] P. Bricage, Survival management of living systems. Keynote, 2nd World Conference on Complex Systems, Agadir, Morocco, 10–12 November 2014.
[39] A. Bejan, Convection Heat Transfer, fourth ed., Wiley, Hoboken, 2013.
[40] A. Bejan, S. Lorente, Design with Constructal Theory, Wiley, Hoboken, 2008, pp. 118–119.
[41] A. Bejan, M.R. Errera, Convective trees of fluid channels for volumetric cooling, Int. J. Heat Mass Transfer 43 (2000) 3105–3118.
[42] A. Bejan, G. Tsatsaronis, M. Moran, Thermal Design and Optimization, Wiley, New York, 1996.
[43] A. Bejan, Why the bigger live longer and travel farther: animals, vehicles, rivers and the winds, Sci. Rep. 2 (2012) 594.
[44] A. Bejan, A. Almerbati, S. Lorente, Economies of scale: The physics basis, J. Appl. Phys. 121 (2017) 044907.